Supporting information

Rising local electron density of carbons for enhanced O_2 activation at room temperature

Yukun Pan [a #], Hai Xu [a #], Lekang Cui[a], Zhiqiang Zhao[a], Weibing Du [c], Jianghao Ye [c], Bo Niu [a], Yayun Zhang,[a,b,] and Donghui Long,[a,b]*

[a] State Key Laboratory of Chemical Engineering, East China University of Science and Technology, Shanghai 200237, China.

[b] Key Laboratory for Specially Functional Materials and Related Technology of the Ministry of Education, East China University of Science and Technology, Shanghai 200237, China

[c] Shanghai Tongzhu Chemical Science & Technology Co., Ltd, Shanghai 200122, China

* Corresponding authors: yy.zhang@ecust.edu.cn (Yayun Zhang)

The author made the same contribution to this work

Supplementary Figures

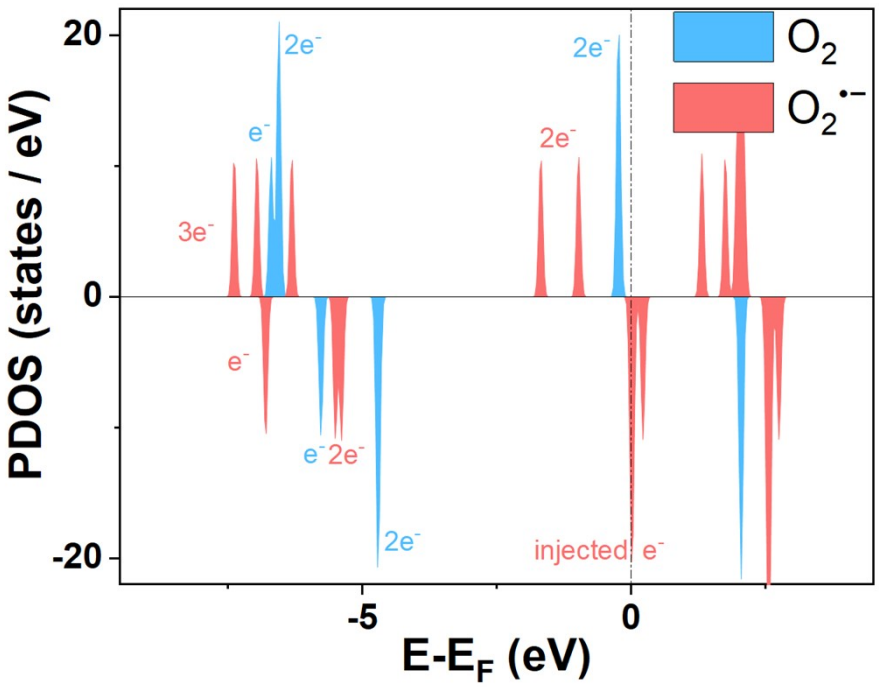

Figure S1. PDOS analysis of $^3O_2$ and $O_2^{\bullet-}$.

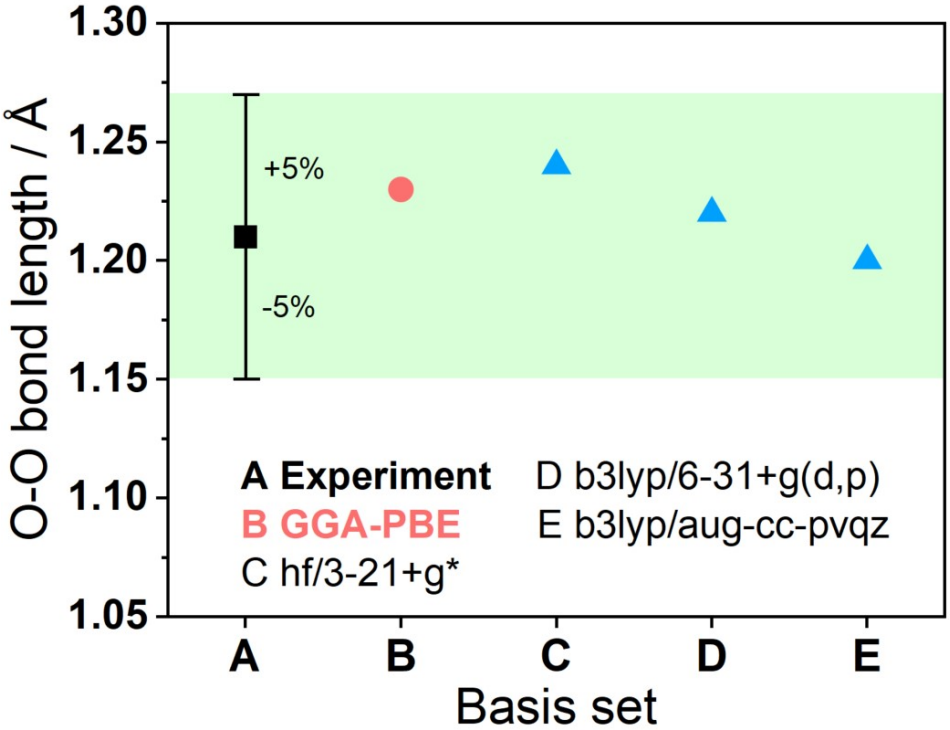

Figure S2 The O-O bond length of O_2 in gas phase calculated by Gaussian and VASP software.

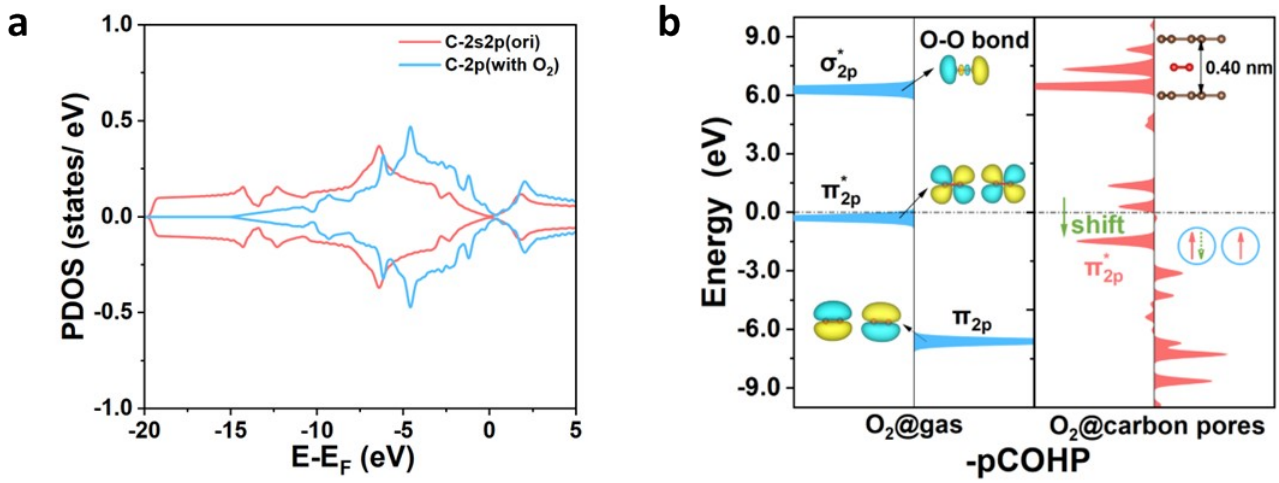

Figure S3. (a) 2s and 2p orbital PDOS of the original sp^2 carbon atom and 2p orbital PDOS of the carbon atom after O_2 enters the ultramicropore. **(b)**COHP of O_2 (g) and O_2 adsorbed in ultramicropore of 4.0 Å.

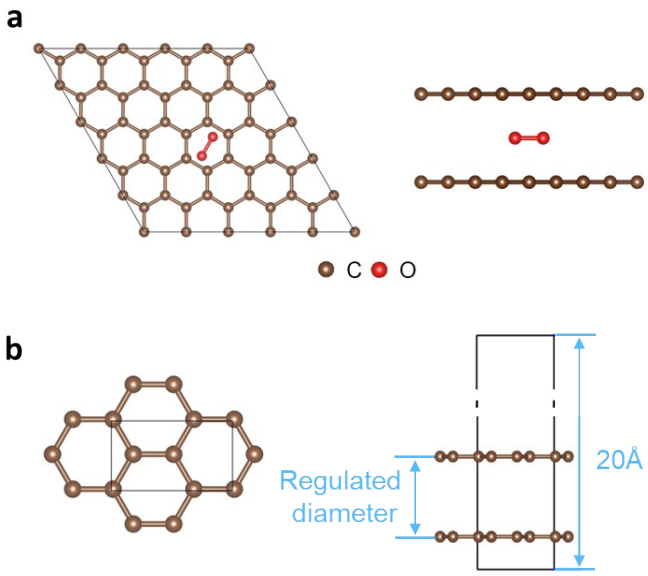

Figure S4 (a) The optimized adsorption conformation of O_2 molecule in slit sp^2 carbon ultramicropore, (top view and main view), (b) The main view and the top view of the sp^2 carbons, and the pore diameter can be regulated from 3.5 Å to 7.0 Å, the vacuum layer is set to 20Å to fully account for the influence of periodicity.

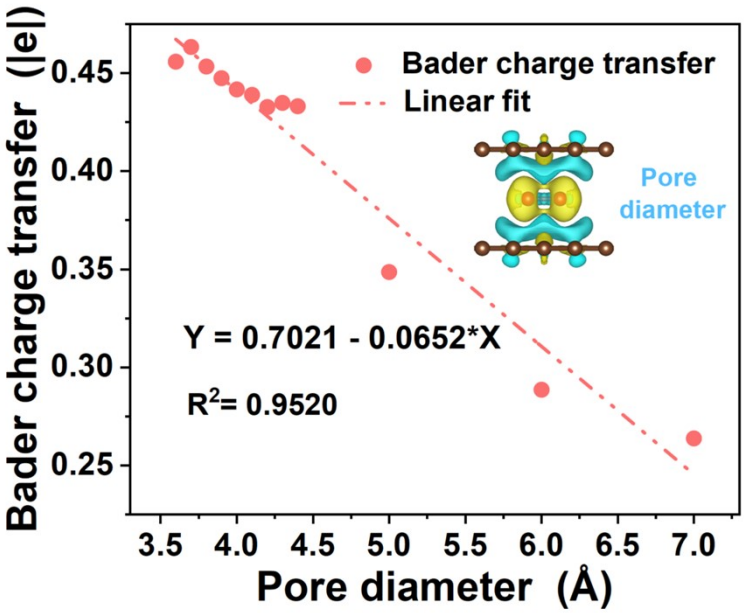

Figure S5. The linear fitting curve with Bader charge transfer (*y*) as the dependent variable and pore diameter (*x*) as the independent variable.

The electron transfer between O_2 and sp^2 carbon has a high negative linear correlation, charge transfer decreases linearly with the pore-diameter increasing, responding to the decay of sub-nanospace confinement.

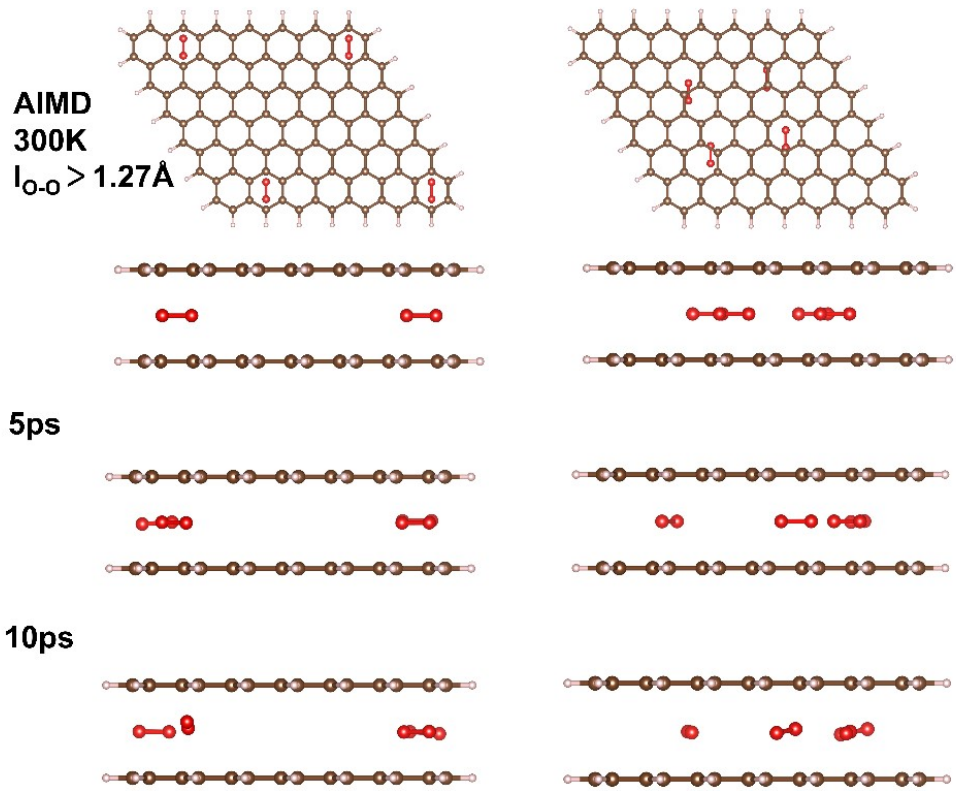

Figure S6. The results of the AIMD simulation were obtained using an aperiodic ultramicropore model, with O_2 positioned at the edge and inside the micropore, respectively.

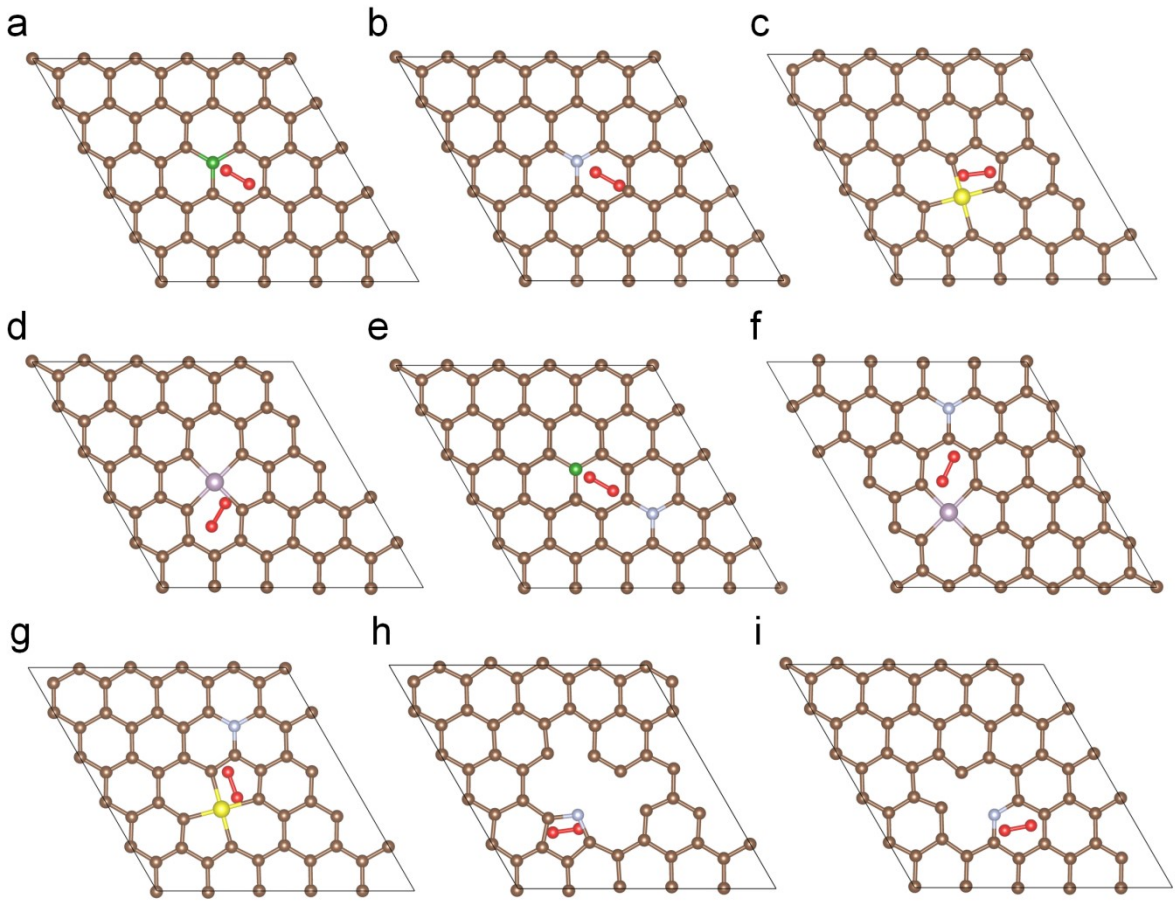

Figure S7. The configurations of absorbed O_2 in non-mental atom doped carbon ultra-micropore, including (a) B atom doping, (b) N atom doping, (c) S atom doping, (d) P atom doping, (e) B-N atoms doping, (f) P-N atoms doping, (g) S-N atoms doping, (h) pyrrole doping (5N-G), (i) pyridine doping (6N-G). Considering the reasonability of theoretical calculations and experiments, the models of thiophene-sulfur (S-G) and four P-C bonds (P-G) were employed to explore their effects on oxygen activation.

Considering the reasonability of theoretical calculations and experiments, the models of thiophene-sulfur (S-G) and four P-C bonds (P-G) were employed to explore their effects on oxygen activation.

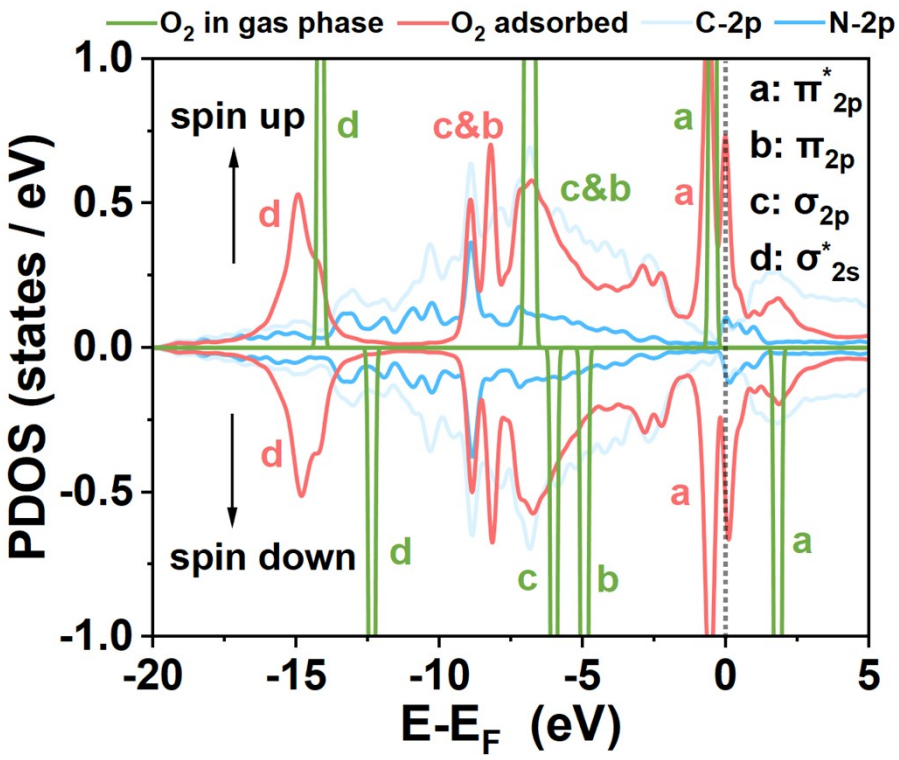

Figure S8. PDOS for O_2 in sp^2 carbon ultra-micropore of graphitic-N doping. The LUMO level of O_2 is lowered to -0.56 eV below the Fermi-level and the gap between HOMO and LUMO is almost reduced to zero, corresponding to the chemical state of $O_2^{\bullet-}$.

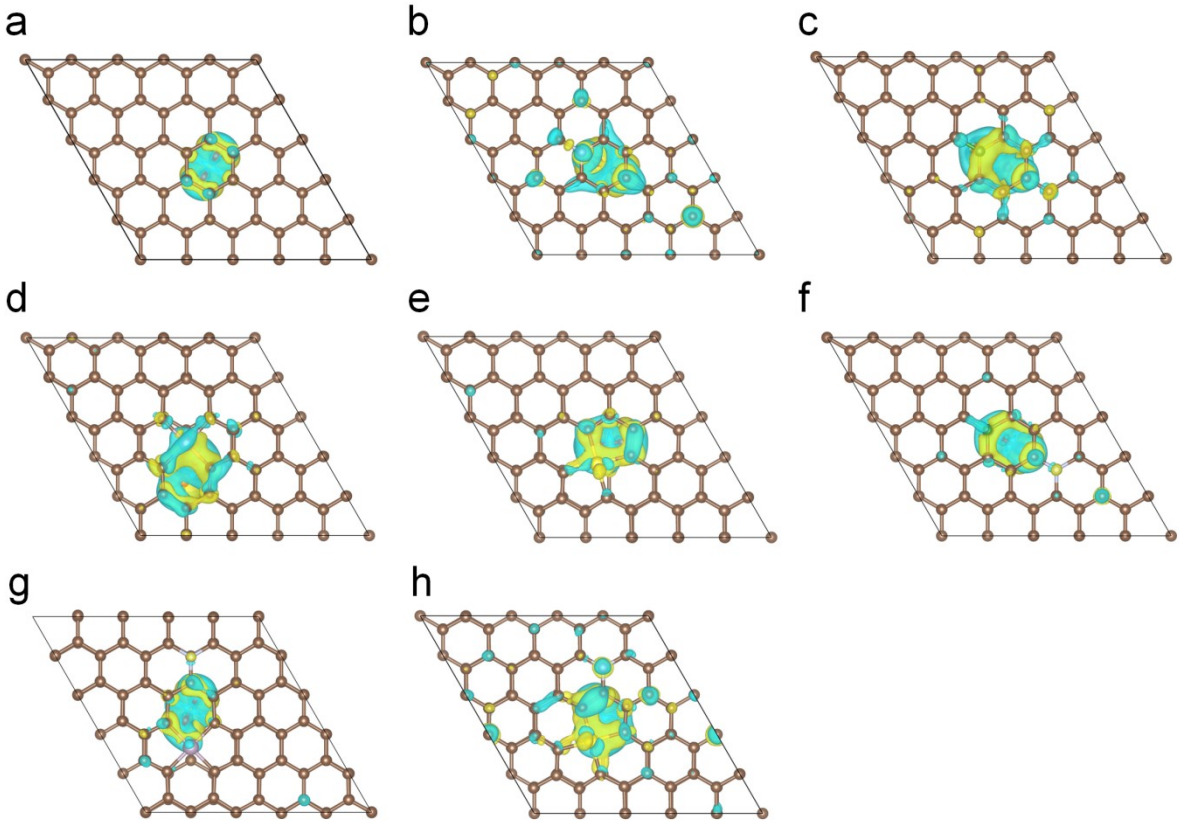

Figure S9. The charge density difference of O_2 adsorbed in non-metal atom doped carbon ultra-micropore, including (a) pristine sp^2 carbon, (b) N atom doped carbon, (c) B atom doped carbon, (d) P atom doped carbon, (e) P atom doped carbon, (f) B-N atoms doped carbon, (g) P-N atoms doped carbon, (h) S-N atoms doped carbon.

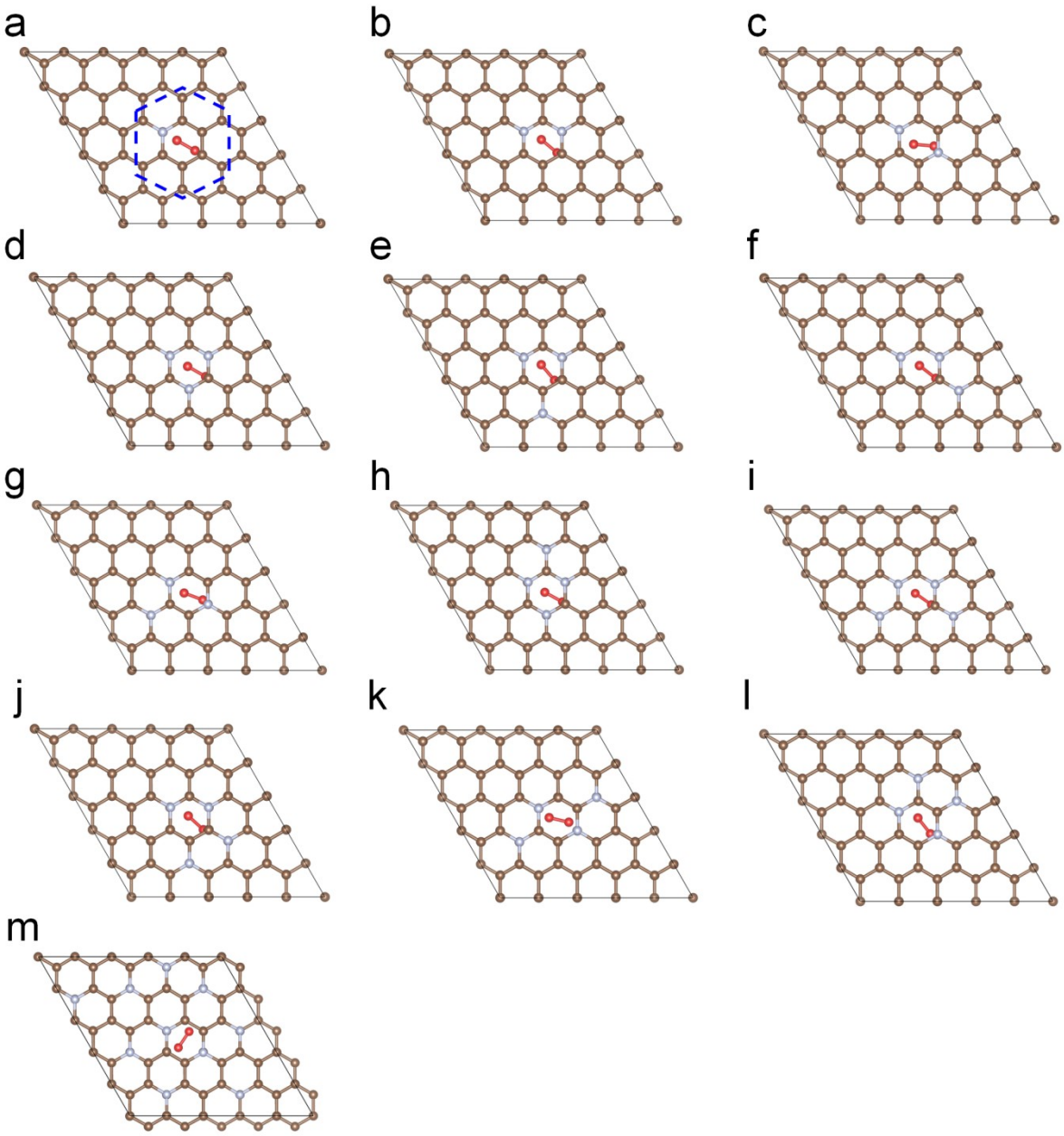

Figure S10. The configurations of top view of absorbed O_2 in different types of graphitic-N doped carbon ultra-micropore with pore diameter of 4.0 Å, and the N doping mass fraction ranges from 0.023 to 0.092.

Regulating the N-doping concentration (N_ω) in the six-membered carbon ring and neighboring carbon totaling 12 atoms at active sites to study the impacts of local nitrogen doping.

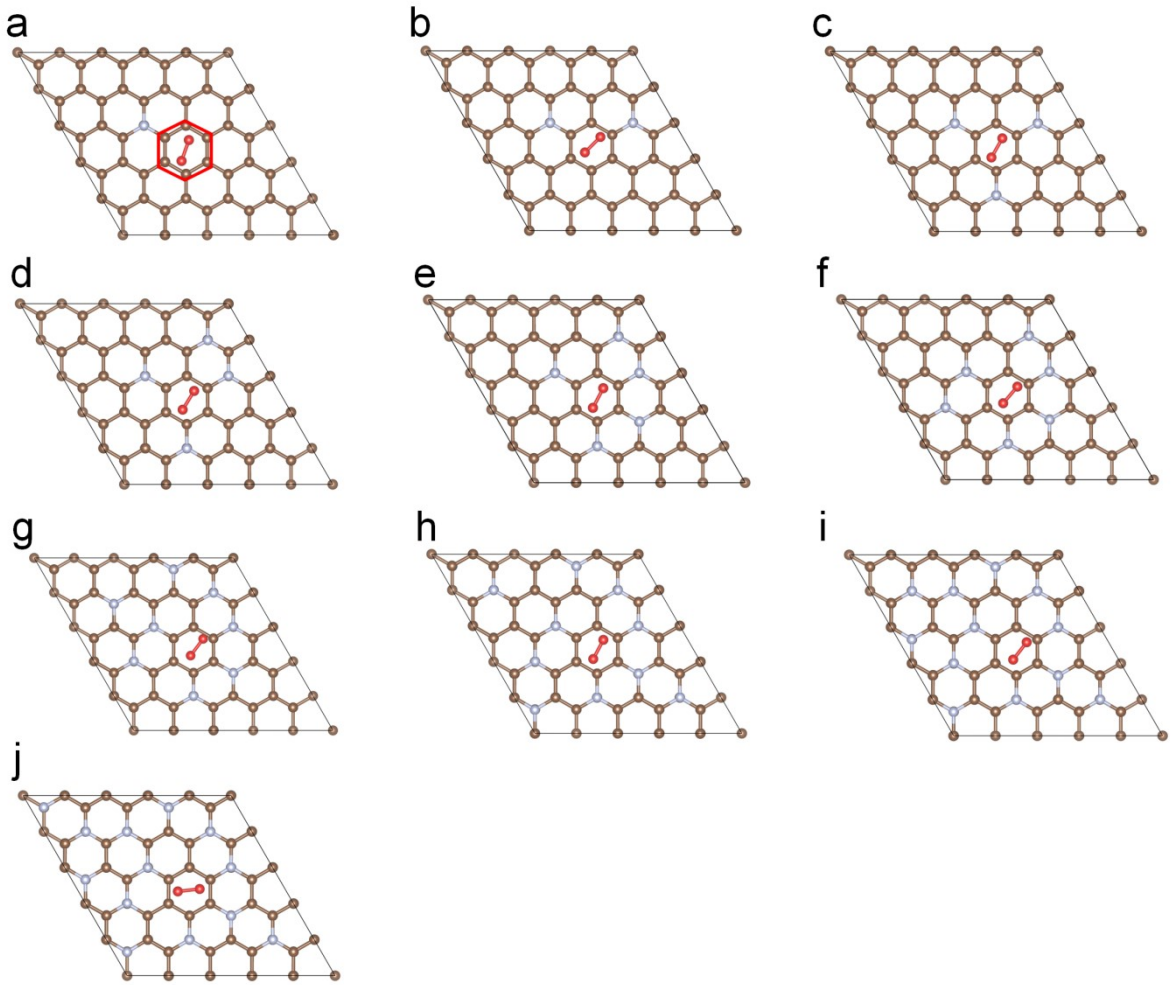

Figure S11. The configurations of top view of absorbed O_2 in graphitic-N doped carbon ultra-micropore with pore-diameter of 4.0 Å, and the N doping mass fraction ranges from 0.023 to 0.291.

We maintained the carbon ring and gradually increased the N doping density over the entire carbons to observe its effect on oxygen activation.

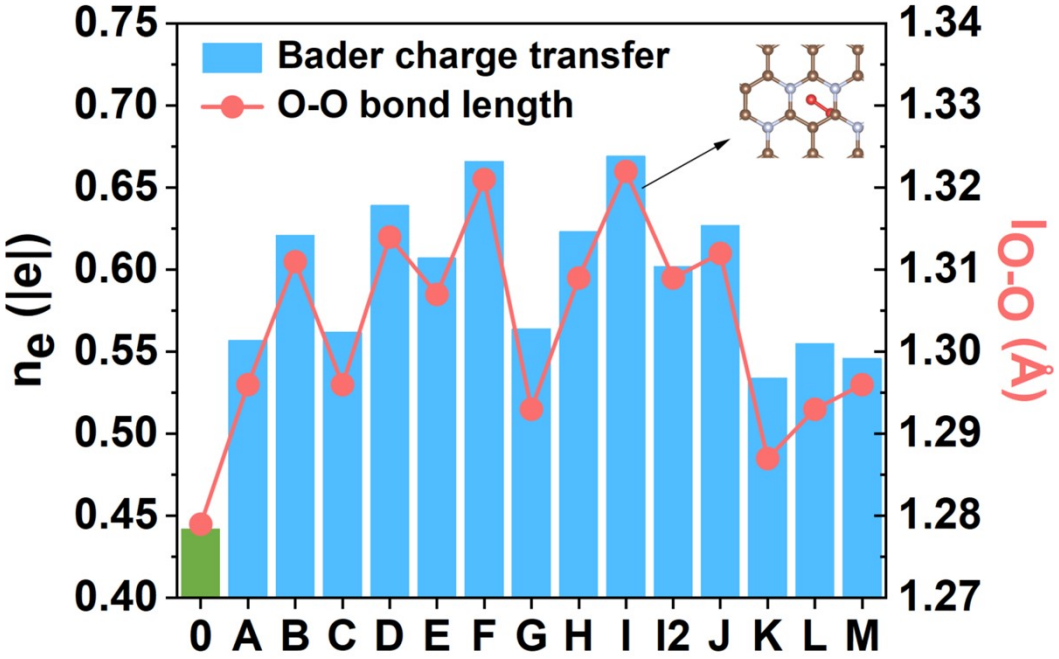

Figure S12. The Bader charge transfer and corresponding O-O bond length of absorbed O_2 in different types of graphitic-N doped carbon ultra-micropore with pore diameter of 4.0 Å, and the N doping mass fraction ranges from 0.023 to 0.092. The letters on the X axis represent different N doping configurations, corresponding to the supporting information in **Figure S11**, and 0 represents the original condition.

The largest charge transfer quantity of O_2 and the longest O-O bond length of O_2 can even reach to 0.67 |e| and 1.32 Å as N_ω is 0.092 (I), far more than that in pure ultra-micropore. The data for I2 is that the pore diameter increases to 4.5 Å.

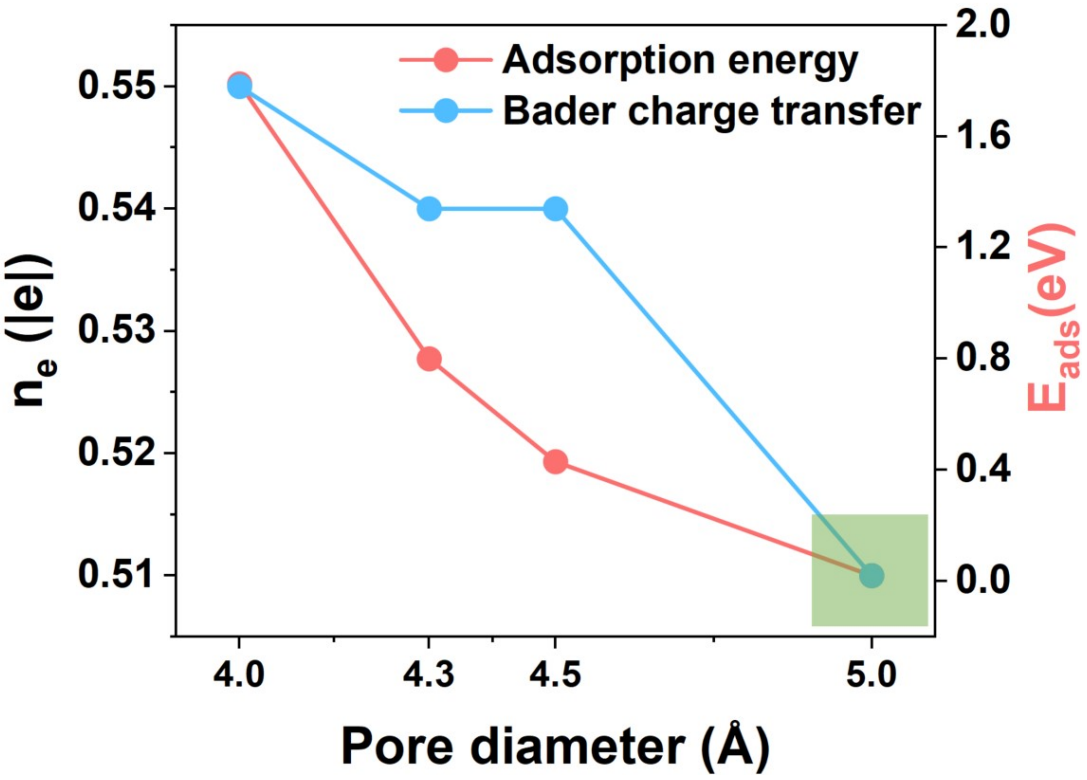

Figure S13. The Bader charge transfer and adsorption energy of adsorbed O_2 in N-doped ultra-micropore (N_ω = 0.092), and the pore diameter is 4.3, 4.5 and 5.0 Å respectively.

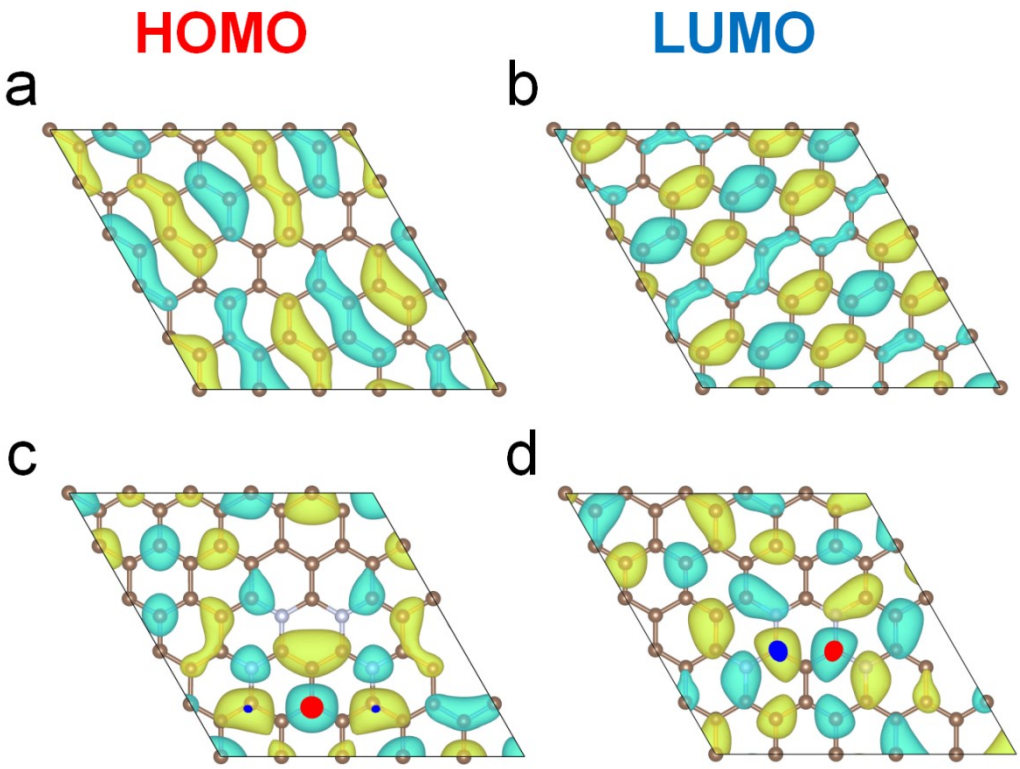

Figure S14. The frontier molecular orbitals (HOMO and LUMO) of non-mental atom doped carbon, including (a-b) pristine sp^2 carbon, (c-d) $C_{46}N_4$.

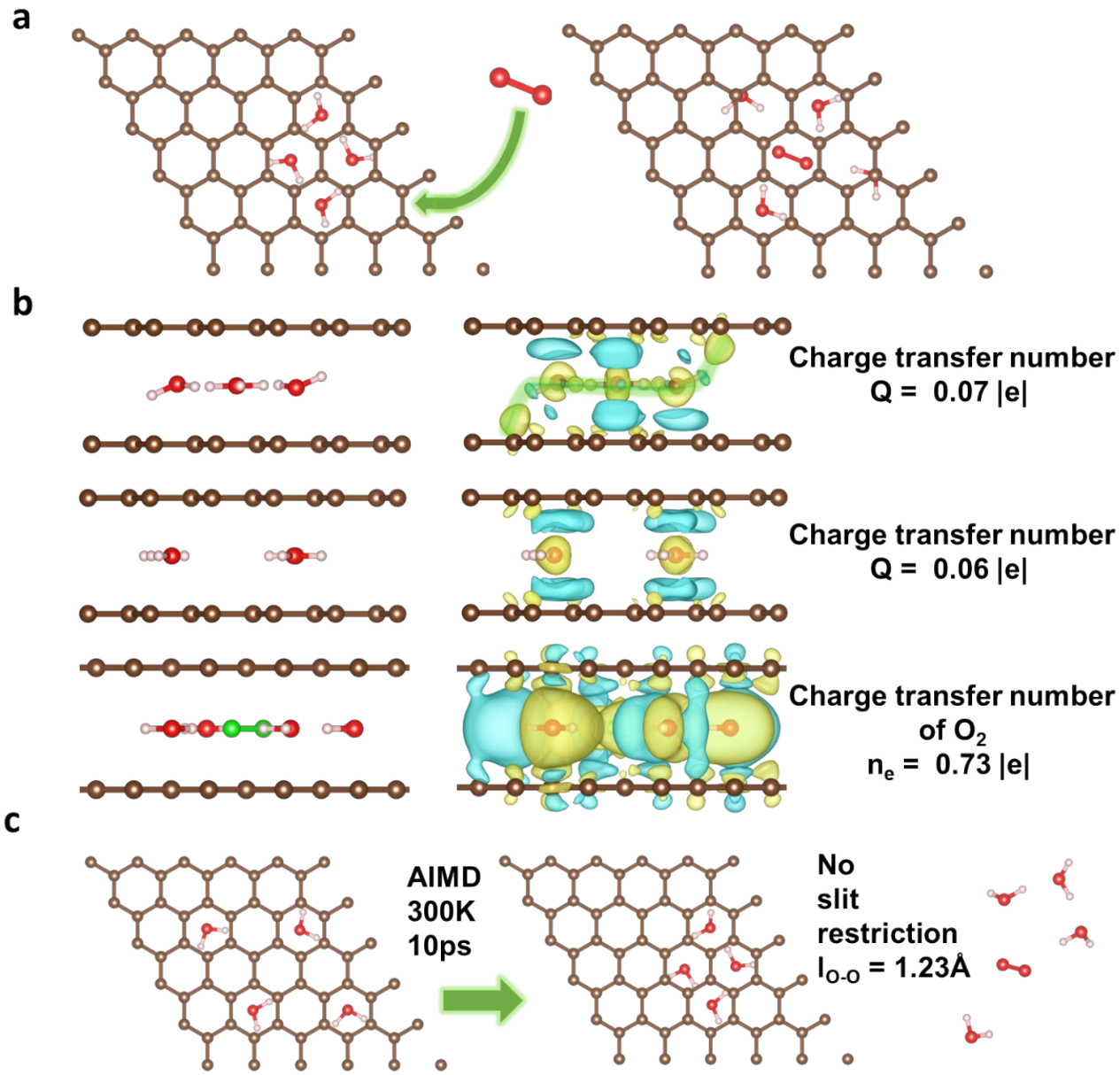

Figure S15. (a) The configuration of H_2O adsorbed in the ultramicropore and the configuration after adding O_2. (b) The charge density difference diagram of 4 H_2O absorbed in the ultramicropore in hydrogen bond aggregation situation and dispersion by O_2 situation, and the charge density difference diagram of coexistence of O_2 and H_2O. (c) The configuration of dispersed H_2O after 10ps AIMD simulation and the optimal structure of H_2O and O_2 molecules without spatial constraints, where O-O bonds are not stretched.

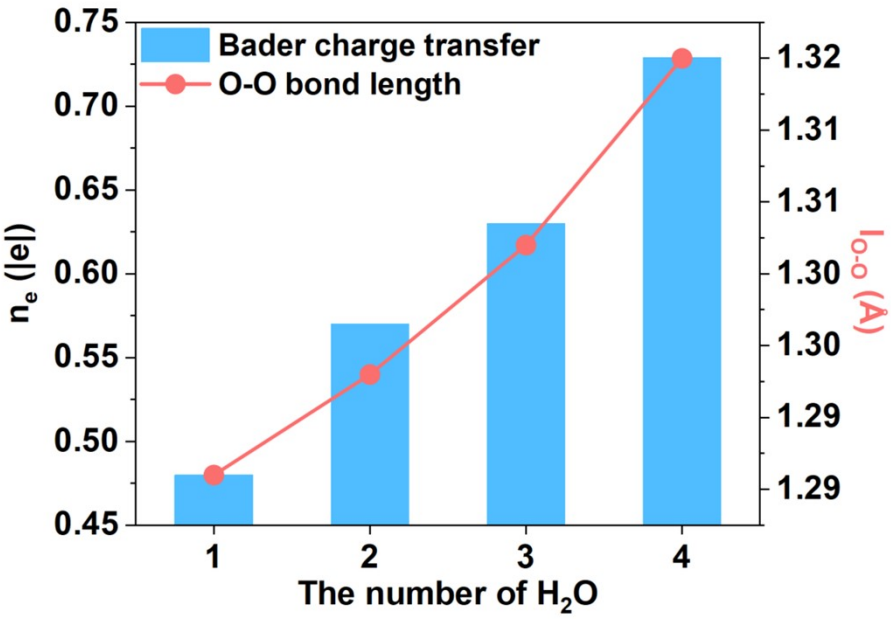

Figure S16. Bader charge transfer and corresponding O-O bond length of adsorbed O_2 with the number of H_2O from 1 to 4.

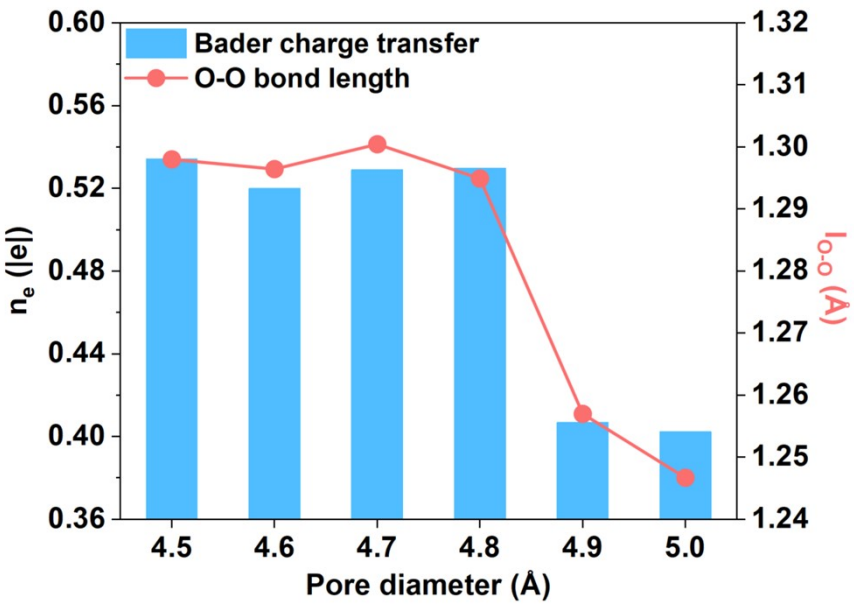

Figure S17. Bader charge transfer and corresponding O-O bond length of O_2 in ultra-micropore of diameter ranging from 4.5Å to 5.0 Å with the effect of two H_2O molecules.

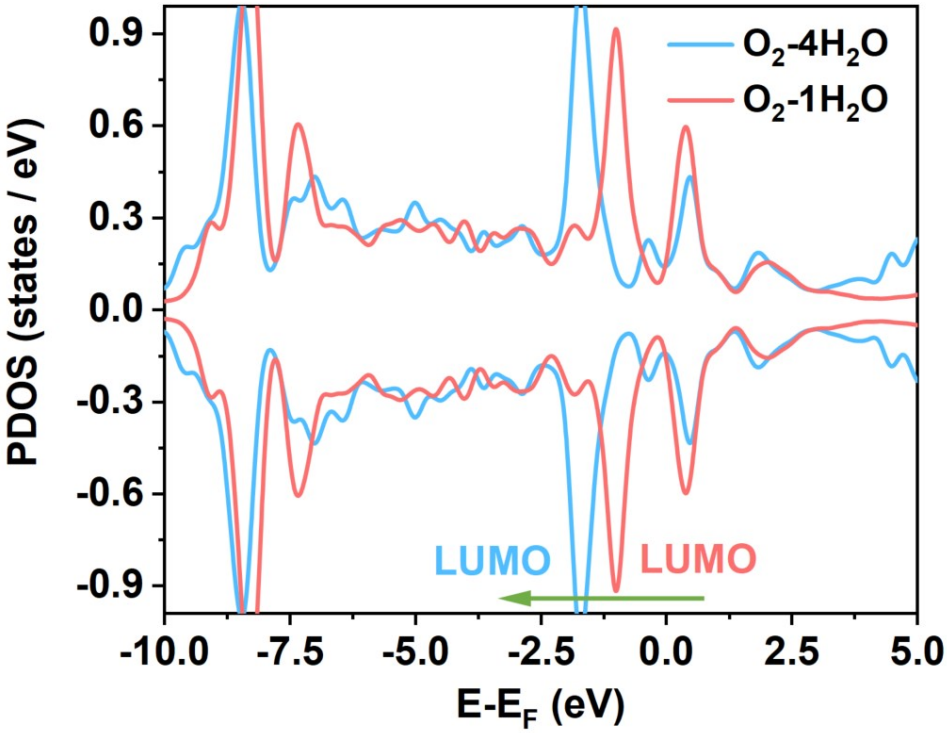

Figure S18. PDOS of O_2 in carbon ultra-micropore of 4.5Å, and the number of H_2O are 1and 4.

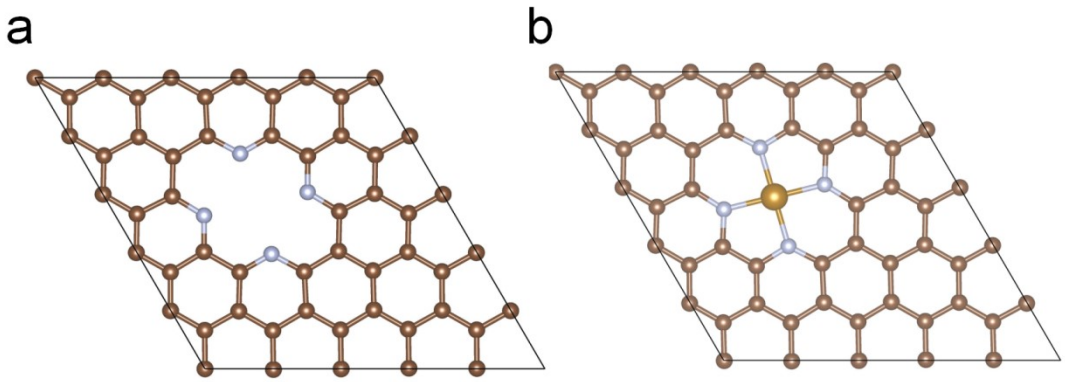

Figure S19. Model of (a) N_4G and (b) Fe-N_4G.

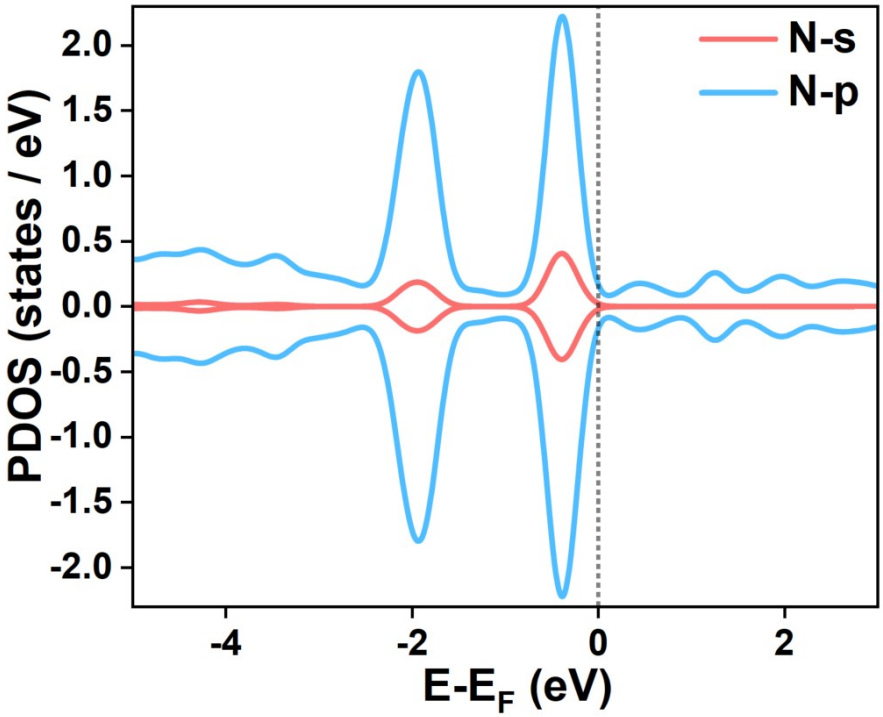

Figure S20. Partial density of states (PDOS) of N_4G

The PDOS of N_4G is characterized by N-p spikes around Fermi-level, and these spikes are related to the lone pair of electrons located on the N atom around the defect site.

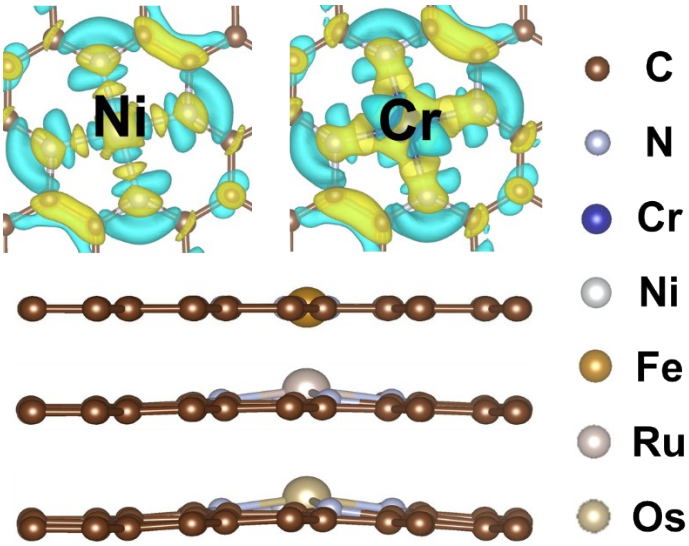

Figure S21. The charge density difference of Cr-N_4G and Ni-N_4G, and the models of single atom material including Fe, Ru and Os.

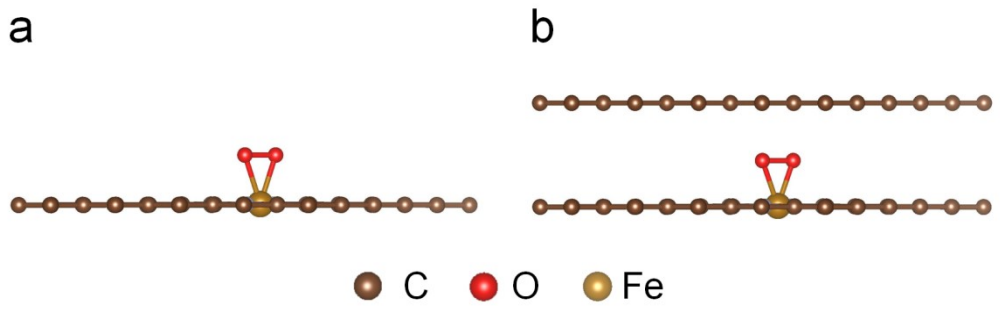

Figure S22. Model of O_2 adsorption on (a) Fe-N_4G without the effect of ultra-micropores, and (b) with the effect of ultra-micropores.

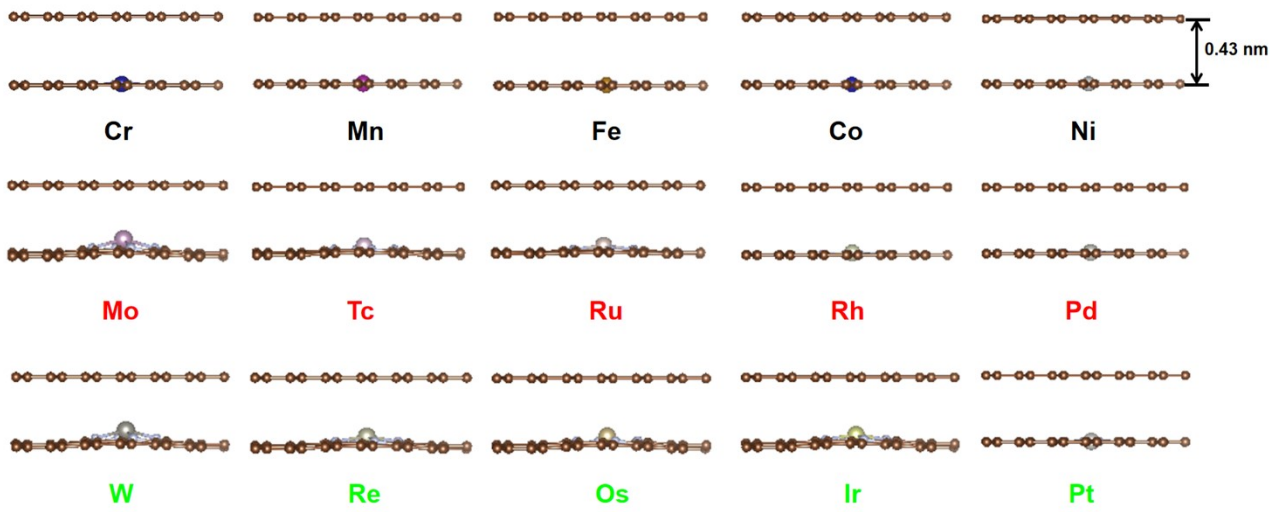

Figure S23. The main view of the molecular model of TM-N_4G composites covering 3d, 4d, and 5d transition metals from VIB to IB group.

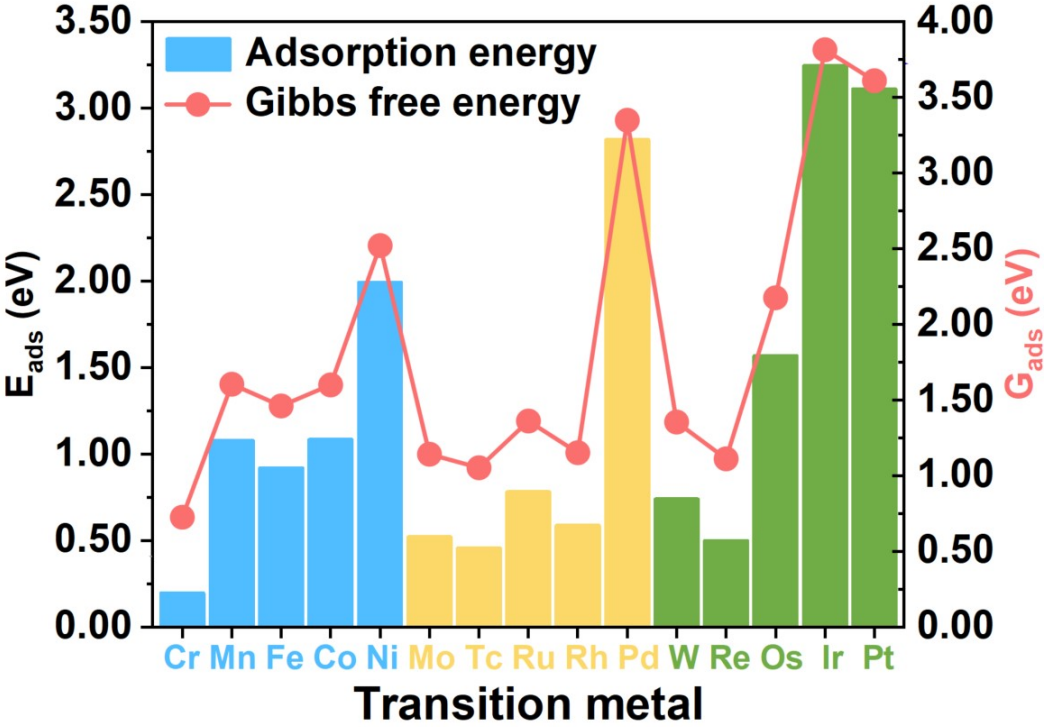

Figure S24. The E_{ads} and corresponding G_{ads} of O_2 on a series of TM-N_4G.

CIF structure information, all the structures given in the document have been modified and re-optimized for the original structure of the cif file.

CONTCAR of ultramicropore (4.0 Å as an example)

```
1.00000000000000
 12.3184995650999998   0.0000000000000000   0.0000000000000000
 -6.1592497825999999  10.6681335598999993   0.0000000000000000
  0.0000000000000000   0.0000000000000000  20.0000000000000000
C    O
100    2
Direct
0.0000000000000000  0.0000000000000000  0.2814899919999974
0.0666700080000027  0.1333300100000017  0.2814899919999974
0.2000000119999967  0.0000000000000000  0.2814899919999974
0.2666699910000006  0.1333300100000017  0.2814899919999974
0.4000000229999969  0.0000000000000000  0.2814899919999974
0.4666700220000024  0.1333300100000017  0.2814899919999974
0.6000000149999991  0.0000000000000000  0.2814899919999974
0.6666700529999972  0.1333300100000017  0.2814899919999974
0.8000000460000010  0.0000000000000000  0.2814899919999974
0.8666700059999997  0.1333300100000017  0.2814899919999974
0.9999999939999995  0.1999999989999992  0.2814899919999974
0.0666700109999994  0.3333300090000009  0.2814899919999974
0.2000000049999997  0.1999999989999992  0.2814899919999974
0.2666699939999972  0.3333300090000009  0.2814899919999974
0.4000000070000027  0.1999999989999992  0.2814899919999974
0.4666700249999991  0.3333300090000009  0.2814899919999974
0.5999999989999978  0.1999999989999992  0.2814899919999974
0.6666700749999990  0.3333300090000009  0.2814899919999974
```

0.8000000689999993	0.1999999989999992	0.2814899919999974
0.8666700289999980	0.3333300090000009	0.2814899919999974
0.9999999870000025	0.3999999979999984	0.2814899919999974
0.0666700270000007	0.5333300519999966	0.2814899919999974
0.1999999989999992	0.3999999979999984	0.2814899919999974
0.2666699999999977	0.5333300519999966	0.2814899919999974
0.4000000099999994	0.3999999979999984	0.2814899919999974
0.4666700309999996	0.5333300519999966	0.2814899919999974
0.5999999830000036	0.3999999979999984	0.2814899919999974
0.6666700430000034	0.5333300519999966	0.2814899919999974
0.8000000139999983	0.3999999979999984	0.2814899919999974
0.8666699959999988	0.5333300519999966	0.2814899919999974
0.0000000020000002	0.6000000189999994	0.2814899919999974
0.0666700000000020	0.7333300290000011	0.2814899919999974
0.2000000130000004	0.6000000189999994	0.2814899919999974
0.2666699919999971	0.7333300290000011	0.2814899919999974
0.4000000249999971	0.6000000189999994	0.2814899919999974
0.4666700229999989	0.7333300290000011	0.2814899919999974
0.6000000169999993	0.6000000189999994	0.2814899919999974
0.6666700540000008	0.7333300290000011	0.2814899919999974
0.8000000480000011	0.6000000189999994	0.2814899919999974
0.8666700079999998	0.7333300290000011	0.2814899919999974
0.9999999739999978	0.7999999950000003	0.2814899919999974
0.0666700120000030	0.9333300050000020	0.2814899919999974
0.1999999860000017	0.7999999950000003	0.2814899919999974
0.2666700039999981	0.9333300050000020	0.2814899919999974
0.3999999979999984	0.7999999950000003	0.2814899919999974
0.4666700349999999	0.9333300050000020	0.2814899919999974

0.5999999900000006	0.7999999950000003	0.2814899919999974
0.6666700660000018	0.9333300050000020	0.2814899919999974
0.8000000210000024	0.7999999950000003	0.2814899919999974
0.8666700189999972	0.9333300050000020	0.2814899919999974
0.0000000000000000	0.0000000000000000	0.0814900040000026
0.0666700080000027	0.1333300100000017	0.0814900040000026
0.2000000119999967	0.0000000000000000	0.0814900040000026
0.2666699910000006	0.1333300100000017	0.0814900040000026
0.4000000229999969	0.0000000000000000	0.0814900040000026
0.4666700220000024	0.1333300100000017	0.0814900040000026
0.6000000149999991	0.0000000000000000	0.0814900040000026
0.6666700529999972	0.1333300100000017	0.0814900040000026
0.8000000460000010	0.0000000000000000	0.0814900040000026
0.8666700059999997	0.1333300100000017	0.0814900040000026
0.9999999939999995	0.1999999989999992	0.0814900040000026
0.0666700109999994	0.3333300090000009	0.0814900040000026
0.2000000049999997	0.1999999989999992	0.0814900040000026
0.2666699939999972	0.3333300090000009	0.0814900040000026
0.4000000070000027	0.1999999989999992	0.0814900040000026
0.4666700249999991	0.3333300090000009	0.0814900040000026
0.5999999989999978	0.1999999989999992	0.0814900040000026
0.6666700749999990	0.3333300090000009	0.0814900040000026
0.8000000689999993	0.1999999989999992	0.0814900040000026
0.8666700289999980	0.3333300090000009	0.0814900040000026
0.9999999870000025	0.3999999979999984	0.0814900040000026
0.0666700270000007	0.5333300519999966	0.0814900040000026
0.1999999989999992	0.3999999979999984	0.0814900040000026
0.2666699999999977	0.5333300519999966	0.0814900040000026

0.4000000099999994	0.3999999979999984	0.0814900040000026
0.4666700309999996	0.5333300519999966	0.0814900040000026
0.5999999830000036	0.3999999979999984	0.0814900040000026
0.6666700430000034	0.5333300519999966	0.0814900040000026
0.8000000139999983	0.3999999979999984	0.0814900040000026
0.8666699959999988	0.5333300519999966	0.0814900040000026
0.0000000020000002	0.6000000189999994	0.0814900040000026
0.0666700000000020	0.7333300290000011	0.0814900040000026
0.2000000130000004	0.6000000189999994	0.0814900040000026
0.2666699919999971	0.7333300290000011	0.0814900040000026
0.4000000249999971	0.6000000189999994	0.0814900040000026
0.4666700229999989	0.7333300290000011	0.0814900040000026
0.6000000169999993	0.6000000189999994	0.0814900040000026
0.6666700540000008	0.7333300290000011	0.0814900040000026
0.8000000480000011	0.6000000189999994	0.0814900040000026
0.8666700079999998	0.7333300290000011	0.0814900040000026
0.9999999739999978	0.7999999950000003	0.0814900040000026
0.0666700120000030	0.9333300050000020	0.0814900040000026
0.1999999860000017	0.7999999950000003	0.0814900040000026
0.2666700039999981	0.9333300050000020	0.0814900040000026
0.3999999979999984	0.7999999950000003	0.0814900040000026
0.4666700349999999	0.9333300050000020	0.0814900040000026
0.5999999900000006	0.7999999950000003	0.0814900040000026
0.6666700660000018	0.9333300050000020	0.0814900040000026
0.8000000210000024	0.7999999950000003	0.0814900040000026
0.8666700189999972	0.9333300050000020	0.0814900040000026
0.5630975173999165	0.5264103455119554	0.1814800814198257
0.5033506338563423	0.4065130139572272	0.1814993274647066